A Complete Mechanism for Steady-State Oxidation of Yeast Cytochrome *c* by Yeast Cytochrome *c* Peroxidase†

Mark A. Miller*

Department of Chemistry and Biochemistry, University of California—San Diego, La Jolla, California 92093-0506

Received June 21, 1996; Revised Manuscript Received September 30, 1996⊗

ABSTRACT: Steady-state oxidation of yeast cytochrome *c* (yC*c*) was monitored as a function of ionic strength (μ) for mutants of a cloned cytochrome *c* peroxidase [C*c*P(MI)]. The data are best interpreted in the context of a two binding site model, where the affinity of the two sites for yC*c* differs by approximately 1000-fold and rapid intracomplex electron transfer (ET) occurs only at the high-affinity site identified in the crystal structure. At low μ, catalysis is apparently limited by the rate of yC*c* dissociation from the reactive high-affinity site (k_{off}). Binding of yC*c* at the low-affinity site increases k_{off} and therefore increases the rate of catalysis. Mutations at the high-affinity site also increase the rate of catalysis by the 1:1 C*c*P(MI):yC*c* complex by increasing k_{off}. Mutations at residues that interact strongly with yC*c* at the high-affinity site (Asp 34, Glu 290, and Ala 193) cause the greatest increase in k_{off} (25−38-fold at μ = 20 mM). Mutations at residues that interact less strongly with yC*c* (Glu 32 and Glu 291) cause smaller increases in k_{off} (10- and 3-fold, respectively, at μ = 20 mM). The results provide additional evidence that the high-affinity site formed in solution is similar to the one identified in the crystal structure and that yC*c* dissociation from this site limits enzyme turnover at low ionic strength. Numerical integration simulations show that the model accurately predicts enzyme turnover rates at the high-affinity site, using published rate constants for the elementary reaction steps.

Cytochrome *c* peroxidase (C*c*P)[1] catalyzes the reduction of peroxide to water. During the catalytic cycle, hydroperoxide reacts with ferric C*c*P to form compound I (eq 1), which retains the oxidizing equivalents of peroxide as a stable oxy-ferryl heme and an indolyl cation radical at Trp 191 [Trp$^{\bullet+}$; for review see English and Tsaprailis (1995)]. The two oxidized sites of compound I are then reduced by two molecules of C*c*^{II} to regenerate the ferric enzyme (eq 2).

$$C\mathit{c}P(Fe^{III}) + HOOH \rightarrow CMPI(Fe^{IV}{=}O;Trp^{\bullet+}) + H_2O \quad (1)$$

$$CMPI(Fe^{IV}{=}O;Trp^{\bullet+}) + 2C\mathit{c}^{II} + 2H^+ \rightarrow C\mathit{c}P(Fe^{III}) + 2C\mathit{c}^{III} + H_2O \quad (2)$$

Electron transfer (ET) from the heme of C*c*^{II} to Trp$^{\bullet+}$ and the oxy-ferryl heme of C*c*P occurs over distances of at least 13 and 19 Å, respectively (Finzel et al., 1984; Pelletier & Kraut, 1992).

A substantial body of kinetic evidence (Geren et al., 1991; Hahm et al., 1992, 1993, 1994; Roe & Goodin, 1993; Liu et al., 1995; Miller et al., 1994; Pappa et al., 1996) indicates that compound I reduction proceeds via initial reduction of the Trp 191 radical, followed by reduction of the oxyferryl heme [this view is not universally held, however; see Matthis and Erman (1995)]. Reduction of the oxy-ferryl heme is dependent upon a readily oxidizable Trp residue at position 191 (Mauro et al., 1988; Miller et al., 1995; Bonagura et al., 1996), and the evidence suggests the reaction mechanism involves an equilibrium between the oxy-ferryl heme and Trp 191, as shown in Scheme 1 (Liu et al, 1994):

Scheme 1

$$CMPI(Fe^{IV}{=}O;Trp^{\bullet+}) + yC\mathit{c}^{II} \rightarrow CMPII(Fe^{IV}{=}O;Trp) + yC\mathit{c}^{III} \quad (3)$$

$$CMPII(Fe^{IV}{=}O;Trp) + H^+ \rightleftarrows CMPII(Fe^{III}\text{-}OH;Trp^{\bullet+}) \quad (4)$$

$$CMPII(Fe^{III}\text{-}OH;Trp^{\bullet+}) + yC\mathit{c}^{II} + H^+ \rightarrow C\mathit{c}P(Fe^{III}) + yC\mathit{c}^{III} + H_2O \quad (5)$$

In this mechanism, intramolecular ET reduces the oxy-ferryl heme and regenerates Trp$^{\bullet+}$ (eq 4) and then intermolecular ET from yC*c*^{II} reduces Trp$^{\bullet+}$ (eq 5). In the crystal structures of the C*c*P:yC*c* and C*c*P:hC*c* complexes, Trp 191 is interposed between the hemes of C*c*P and C*c* (Pelletier & Kraut, 1992), a configuration that is consistent with Scheme 1. Recent evidence indicates that the predominant C*c*P(MI):C*c* complex formed in solution is similar to the crystal structure (Miller et al., 1994, 1996; J. E. Erman, unpublished observations), and that ET occurs only at this binding site (Miller et al., 1996). A readily oxidized Trp 191 is required for rapid reduction of compound I, consistent with the

† Supported by NSF Grant MCB 94-29845.

⊗ Abstract published in *Advance ACS Abstracts,* November 15, 1996.

[1] Abbreviations: C*c*P, cytochrome *c* peroxidase from yeast *Saccharomyces cerevisiae*; C*c*P(MI), a cloned C*c*P expressed in *Escherichia coli*; CMPI = compound I, the two-electron oxidation product of the reaction of ferric C*c*P with hydrogen peroxide; CMPII = compound II, the one-electron reduction product formed by reaction of compound I with one molecule of C*c*^{II}; Fe^{IV}=O, oxy-ferryl heme; Trp$^{\bullet}$, the indolyl radical formed at Trp 191 of C*c*P; yC*c*, cytochrome *c* from yeast *S. cerevisiae*; hC*c*, cytochrome *c* from horse; Zn-C*c*P, Zn-C*c*, cytochrome *c* peroxidase and cytochrome *c* which have the native heme replaced by a zinc porphyrin; Ru-39-yC*c*, cytochrome *c* from yeast with a ruthenium (bipy)$_2$(4,4′-dimethylbipyridine) moiety attached to an engineered Cys at position 39; MPB, 3-(*N*-maleimidylpropionyl)-biocytin; μ, ionic strength; ET, electron transfer; NMR, nuclear magnetic resonance spectroscopy.

S0006-2960(96)01488-2 CCC: $12.00

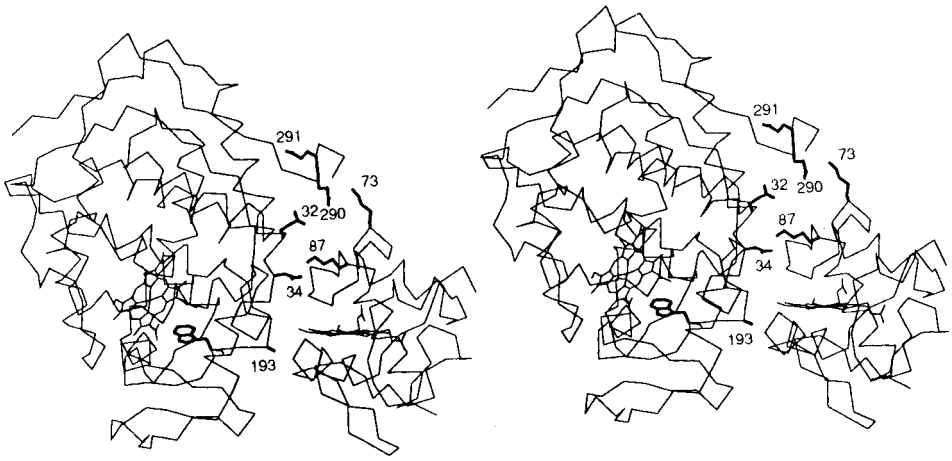

FIGURE 1: Stereoview of the interface between C*c*P(MI) and yC*c*. The α-carbon traces for C*c*P and yC*c* are shown in thin lines, and the side chains of mutation sites, Trp 191 of C*c*P(MI), and important Lys residues of yC*c* are shown with bold lines. Data are from Pelletier and Kraut (1992).

reaction shown in eq 4 (Mauro et al., 1988; Liu et al., 1994, 1995, Miller et al., 1995; Bonagura et al., 1996).

The one binding site mechanism of Scheme 1 is not entirely satisfactory because enzyme turnover (k_{cat}) at low ionic strength exceeds the rate of yCc^{III} dissociation from the high-affinity binding site (Yi et al., 1994). This observation suggests that the second, low-affinity binding site for yC*c* (Kornblatt & English, 1986; Mauk et al., 1994; Stemp & Hoffman, 1993; Zhou & Hoffman, 1994; Zhou et al., 1995) must also be involved in catalysis. It has generally been assumed that a significant percentage of the total ET at low ionic strength occurs via the second, low-affinity binding site (Matthis & Erman, 1995; Matthis et al., 1995; Zhou & Hoffman, 1994; Pappa & Poulos, 1995; Wang & Margoliash 1995), but this assumption is in conflict with recent evidence that only the high-affinity binding site is reactive in physiological ET (Miller et al., 1996).

To investigate this discrepancy further, steady-state oxidation of yCc^{II} was examined in several point mutants of a cloned C*c*P [C*c*P(MI); Fishel et al., 1987] that perturb the high affinity C*c*P:yC*c* complex (Miller et al., 1994). Each of the mutants has a single residue substitution in one of the three regions that contact yC*c* in the crystal structure of the C*c*P:yC*c* complex (Figure 1; Pelletier & Kraut, 1992). Two of these residues, Glu 290 and Asp 34, have carboxylate side chains within 4 Å of the ϵ-amino groups of Lys 73 and Lys 87 of yC*c*, respectively. The Glu 290 → Asn and Asp 34 → Asn mutations were created to eliminate these complementary charge:charge interactions. A third residue, Ala 193, is only 4 Å from the yC*c* heme. The Ala 193 → Phe mutation was designed to create steric conflict between Phe 193 of C*c*P(MI) and Gln 16 of C*c* in the crystal structures.[2] To discriminate between general and specific effects of charge neutralization, two other carboxylate residues were modified. The Glu 32 → Gln mutation neutralizes a carboxylate residue that is 5 Å from Lys 87 of yC*c*, while the Glu 291 → Gln mutation neutralizes a carboxylate side chain that projects away from the interface with yC*c*. Based on the crystal structure, the affinity of these enzymes for yC*c* is expected to decrease in the order C*c*P(MI) > C*c*P(MI,Q291) > C*c*P(MI,Q32) > C*c*P(MI,N34) = C*c*P(MI,F193) = C*c*P(MI,N290), as observed for the closely related complex formed by C*c*P(MI) and horse cytochrome *c* (hC*c*) (Liu et al., 1995; J. E. Erman, unpublished observations).

EXPERIMENTAL PROCEDURES

Materials. Cytochrome *c* from yeast (Sigma) was used without further purification. All other materials were of reagent grade or better.

Mutant Enzymes. Mutations were introduced into the coding sequence of a cloned cytochrome *c* peroxidase gene [C*c*P(MI)] as described (Fishel et al., 1987; Miller et al., 1994). The enzymes were expressed in 15 L cultures of *Escherichia coli* strain SK383, converted to the holo-enzyme, and purified to homogeneity as described (Fishel et al., 1987). The absorption spectra of all mutants reported here were within experimental error of the C*c*P(MI) parent ($\epsilon_{408} = 102$ mM^{-1} cm^{-1} in 100 mM potassium phosphate buffer, pH 6.0, 25 °C).

Steady-State Kinetics. The protocol for steady state activity measurement has been described elsewhere (Miller et al., 1995). Solutions of yCc^{II} used for kinetic experiments contained no more than 5% yCc^{III}. Kinetic measurements were conducted in 5 mM sodium phosphate buffer, pH 6.0, brought to the desired ionic strength by adding a calculated amount of NaCl. For each condition, measurements were made at four enzyme concentrations. The data traces were best fit by an equation describing two decay processes: one was first order in yC*c* concentration and linearly dependent upon enzyme concentration, while the other was second order in yC*c* concentration and independent of enzyme concentration. The value of v_0 was calculated as the best linear fit of initial rate versus enzyme concentration. Reproducibility was typically ±5% on any given day, and ±10% from day to day. Reported values of v_0 were corrected for two molecules of yCc^{II} oxidized per enzyme turnover, i.e., $v_0 = {}^1/_2(d[Cc^{II}]/dt)$.

Data Analysis. Because a non-hyperbolic dependence of v_0 on yCc^{II} concentration has been reported (Matthis &

[2] The Ala 193 → Phe mutation was expected to decrease the affinity of C*c*P(MI) for C*c* by introducing a close contact between the Phe side chain at position 193 and Gln 16 of C*c*. Recent calorimetric studies confirm that this substitution decreases the affinity of C*c*P(MI) for hC*c*, but it does not alter the change in enthalpy of C*c*P(MI):hC*c* complex formation (J. E. Erman, unpublished observations). Thus, in the case of hC*c*, the decreased affinity is most likely caused by an increase in the entropy of C*c*P(MI) rather than a steric conflict with Gln 16 of hC*c*.

Table 1: Kinetic Parameters for High Affinity Kinetic Process of C*c*P(MI) and Mutants[a]

μ	C*c*P(MI)		Q291		Q32		N34		F193		N290	
(mM)	k_{cat1} (s^{-1})	K_{m1} (μM)	k_{cat1} (s^{-1})	K_{m1} (μM)	k_{cat1} (s^{-1})	K_{m1} (μM)	k_{cat1} (s^{-1})	K_{m1} (μM)	k_{cat1} (s^{-1})	K_{m1} (μM)	k_{cat1} (s^{-1})	K_{m1} (μM)
20	5 ± 2	$\ll 0.1$	14 ± 2	$\ll 0.1$	50 ± 4	$\ll 0.1$	138 ± 10	0.1 ± 0.1	127 ± 5	0.31 ± 0.08	189 ± 11	<0.2
30	25 ± 6	$\ll 0.1$			160 ± 10	0.8 ± 0.3	386 ± 32	0.8 ± 0.1	400 ± 21	1.4 ± 0.3	459 ± 26	0.5 ± 0.1
40	49 ± 2	$\ll 0.1$									772 ± 30	1.0 ± 0.3
50	130 ± 6	0.16 ± 0.05	229 ± 18	1.3 ± 0.5	556 ± 40	2.2 ± 0.5	828 ± 20	2.8 ± 0.3	1122 ± 16	2.7 ± 0.2		
75	456 ± 20	1.0 ± 0.1			1097 ± 125	8 ± 2						
90	692 ± 30	2.3 ± 0.3										
110	1189 ± 27	5.8 ± 0.5	1530 ± 39	5.4 ± 0.5	2300 ± 90	19 ± 2	893 ± 29	24 ± 2	1490 ± 50	18 ± 2	1963 ± 83	24 ± 2
125	1600 ± 30	8.2 ± 0.5										
140	2009 ± 74	24 ± 2										
160	2123 ± 141	55 ± 5										
200	2000 ± 180	65 ± 10										

[a] Kinetic data were obtained in 5 mM sodium phosphate buffer, pH 6.0, 25 °C, brought to the indicated ionic strength with NaCl. Kinetic parameters derived from the best fit of the data to eq 6 and are expressed ± standard error (for details, see Experimental Procedures).

Table 2: Kinetic Parameters for Low-Affinity Kinetic Process of C*c*P(MI) and Mutants[a]

μ	C*c*P(MI)		Q291		Q32		N34		F193		N290	
(mM)	k_{cat2} (s^{-1})	K_{m2} (μM)	k_{cat2} (s^{-1})	K_{m2} (μM)	k_{cat2} (s^{-1})	K_{m2} (μM)	k_{cat2} (s^{-1})	K_{m2}(μM)	k_{cat2} (s^{-1})	K_{m2}(μM)	k_{cat2} (s^{-1})	K_{m2} (μM)
20	319 ± 45	122 ± 29	159 ± 44	46 ± 20	364 ± 127	127 ± 70	688 ± 141	104 ± 38	–	–	812 ± 314	109 ± 78
30	361 ± 100	115 ± 55	–	–	–	–	–	–	–	–	–	–

	k_{cat2}/K_{m2} ($\times 10^{-6}$ M^{-1} s^{-1})	k_{cat2}/K_{m2} ($\times 10^{-6}$ M^{-1} s^{-1})	k_{cat2}/K_{m2} ($\times 10^{-6}$ M^{-1} s^{-1})	k_{cat2}/K_{m2} ($\times 10^{-6}$ M^{-1} s^{-1})	k_{cat2}/K_{m2} ($\times 10^{-6}$ M^{-1} s^{-1})	k_{cat2}/K_{m2} ($\times 10^{-6}$ M^{-1} s^{-1})
20	–	–	–	–	5.9 ± 0.2	–
30	–	–	1.8 ± 0.1	3.8 ± 0.3	6.3 ± 0.4	4.6 ± 0.5
40	1.8 ± 0.1	–	4.2 ± 1.1	–	–	5.3 ± 1.1
50	1.7 ± 0.1	1.7 ± 0.4	4.4 ± 1.4	nd	nd	–
75	1.8 ± 0.1	–	2.6 ± 1.5	–	–	–
90	1.8 ± 0.5	–	–	–	–	–
110	nd[b]	nd	nd	nd	nd	nd

[a] Kinetic data were obtained in 5 mM sodium phosphate buffer, pH 6.0, 25 °C, and brought to the indicated ionic strength with NaCl. Kinetic parameters derived from the best fit of the data to eq 6 and are expressed ± standard error (for details, see Experimental Procedures). [b] nd, not determined.

Erman, 1995; Wang & Margoliash, 1995; Kang et al., 1977; Miller et al., 1996), the data were analyzed assuming one or two saturable processes may be present under these conditions. The general form of the fit is

$$v_0 = \frac{k_{catl}[Cc^{II}]}{K_{ml} + [Cc^{II}]} + \frac{k_{cat2}[Cc^{II}]}{K_{m2} + [Cc^{II}]} \qquad (6)$$

For a single binding site mechanism, a simple hyperbolic substrate-dependence is expected, i.e., $k_{cat2} = 0$. If two binding sites are involved, the substrate dependence may take the form of two hyperbolas (i.e., k_{cat1}; $k_{cat2} \neq 0$). Equation 6 has two limiting forms: if $[Cc^{II}] \gg K_{m1}$, the substrate dependence will appear as a rectangular hyperbola with a non-zero intercept; and if $[Cc^{II}] \ll K_{m2}$, the substrate dependence will appear as the sum of a rectangular hyperbola and a straight line. All four possible cases were considered in analyzing the data for each of the mutants characterized here. The parameters reported in Tables 1 and 2 were derived by finding the best fit of the data to two, three, or four parameter fits, using a commercially available software package which employs a modification of the Marquardt (1963) algorithm. The standard error for each parameter was estimated by the matrix inversion method (Bevington & Robinson, 1992).

RESULTS

The kinetics of yCc^{II} oxidation by the mutants was examined between $\mu = 20$ mM and $\mu = 110$ mM. The ionic strength dependence of yCc^{II} oxidation for all of the mutants is qualitatively similar to the C*c*P(MI) parent (Miller et al., 1996). At high ionic strength ($\mu \geq 110$ mM) the yCc^{II} dependence of the initial rate of yCc^{II} oxidation (v_0) conforms to a simple hyperbola and can be described by two parameters, k_{cat1} and K_{m1}. As the ionic strength decreases from $\mu = 110$ mM to $\mu = 20$ mM, a second kinetic process is detected. At the highest ionic strengths where it is detected, the second process appears non-saturable, and the yCc^{II} dependence of v_0 is best described as the sum of a hyperbola and a line. The hyperbolic process is defined by the parameters k_{cat1} and K_{m1}, while the linear process is described by the parameter k_{cat2}/K_{m2}. As the ionic strength is decreased further, the second process exhibits saturation behavior. At $\mu = 20$ mM, the data for C*c*P(MI), C*c*P(MI,Q291), and C*c*P(MI,Q32) are most accurately described as a hyperbola with a non-zero *Y*-intercept (Figure 2). The hyperbola is defined by the parameters k_{cat2} and K_{m2}, while the *Y*-intercept is defined as k_{cat1} (see below). The data for C*c*P(MI,N34), C*c*P(MI,N290), and C*c*P(MI,F193) are best described as the sum of two hyperbolas, defined by the four parameters k_{cat1}, K_{m1}, k_{cat2}, and K_{m2} in eq 6. The relevant parameters derived from these experiments are collected in Tables 1 and 2.

It is assumed here that k_{cat} and K_m will vary continuously with ionic strength if these parameters describe a single process. For example, both k_{cat1} and K_{m1} decrease monotonically for C*c*P(MI) as the ionic strength decreases from $\mu = 200$ mM to $\mu = 50$ mM (Figure 3A,B), and it is assumed that this reflects the influence of ionic strength on a single

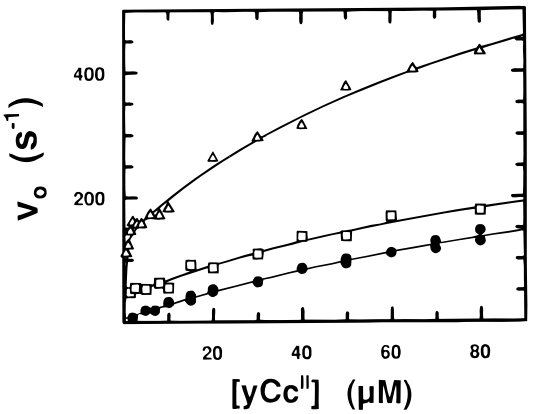

FIGURE 2: yC*c*^{II} dependence of the initial rate of yC*c*^{II} oxidation by C*c*P(MI), C*c*P(MI,Q32), and C*c*P(MI,N34) at $\mu = 20$ mM. The buffer system was 5 mM sodium phosphate, pH 6.0, adjusted to 20 mM with NaCl, 25 °C. Solid circles, C*c*P(MI); open squares, C*c*P(MI,Q32); open triangles, C*c*P(MI,N34). The lines are best fits of the data for C*c*P(MI) and C*c*P(MI,Q32) to the three-parameter (hyperbola with a non-zero intercept) and C*c*P(MI,N34) to the four-parameter (two hyperbolas) model described in eq 6 under Experimental Procedures. The relevant parameters for each fit are given in Tables 1 and 2.

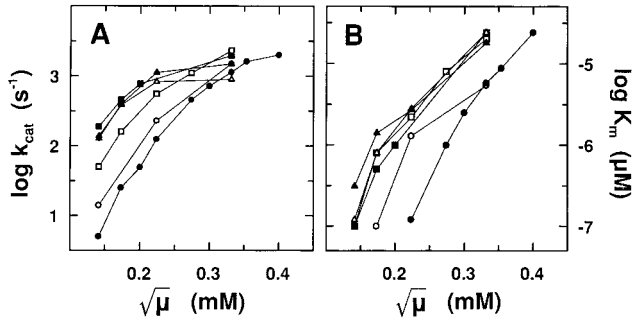

FIGURE 3: Ionic strength dependence of steady-state parameters k_{cat1} and K_{m1} for C*c*P(MI) and mutants. Experiments were conducted as described under Experimental Procedures in 5 mM sodium phosphate buffer, pH 6.0, 25 °C, with sufficient NaCl added to bring the buffer to the indicated ionic strength. C*c*P(MI), closed circles; C*c*P(MI,Q291), open circles; C*c*P(MI,Q32), open squares; C*c*P(MI,N34), open triangles; C*c*P(MI,F193), closed triangles; C*c*P(MI,N290), closed squares.

kinetic process. The data presented in Figure 3B makes it possible to predict that when $\mu < 50$ mM, $K_{m1} \ll 0.2$ μM for C*c*P(MI). Thus, when $\mu < 50$ mM, the process described by k_{cat1} and K_{m1} will be saturated at the lowest yC*c*^{II} concentration employed, and k_{cat1} will be given by the *Y*-intercept observed in plots of v_0 vs yC*c*^{II} concentration. The values of k_{cat1} derived in this way are continuous with those observed when $\mu \geq 50$ mM (Figure 3A), and it is therefore assumed that the parameters k_{cat1} and K_{m1} (Table 1) describe a single kinetic process that involves yC*c* binding at the high-affinity site of C*c*P(MI).

By similar logic, it is assumed that the process described by k_{cat2} and K_{m2} when $\mu \leq 30$ mM is the same one described by k_{cat2}/K_{m2} at higher ionic strength (Table 2). This process is presumed to depend upon formation of a low-affinity complex between C*c*P and yC*c*. At high ionic strength, saturation is not detected, presumably because yC*c* binding at the low-affinity site is weaker at high ionic strength (i.e., $K_{m2} \gg 80$ μM). This is consistent with previous results (Mauk et al., 1994; Mei et al., 1996). At low ionic strength, binding at this site is stronger and saturation can be detected in the concentration range of yC*c*^{II} employed here. This is the predicted effect of ionic strength upon complex formation between molecules of opposite charge. There is not a pronounced effect of ionic strength upon K_{m2} or k_{cat2}/K_{m2}, however (Table 2). This may indicate that ionic strength has a weaker effect on yC*c* binding at the low-affinity site than on binding at the high-affinity site, as predicted by Matthis and Erman (1995). More accurate determinations of these parameters will be required to clarify this point.

The high- and low-affinity processes observed for C*c*P(MI) are also observed for each of the mutant enzymes. As the ionic strength decreases from $\mu = 110$ mM to $\mu = 20$ mM, k_{cat1} and K_{m1} decrease monotonically as a function of ionic strength for each mutant enzyme (Figure 3A,B). As the ionic strength decreases, the low-affinity process becomes apparent. This process exhibits a linear dependence on yC*c*^{II} when $\mu > 30$ mM and a hyperbolic dependence upon yC*c*^{II} when $\mu = 20$ mM.

The effect of individual mutations on the high-affinity process are revealed by changes in k_{cat1} and K_{m1}. At $\mu = 20$ mM, the *Y*-intercept (k_{cat1}) for C*c*P(MI,Q291) increases 3-fold relative to C*c*P(MI), while k_{cat1} for C*c*P(MI,Q32) increases 10-fold (Figure 2). Mutations at Asp 34, Ala 193, and Glu 290 cause even larger effects. Each of these mutations increases the apparent K_{m1} to measurable values (Table 2; Figure 2), and k_{cat1} for C*c*P(MI,N34), C*c*P(MI,F193), and C*c*P(MI,N290) is 25-, 27-, and 36-fold greater than C*c*P(MI), respectively.

As with C*c*P(MI), the value of k_{cat1} for the mutants has a strong dependence upon ionic strength. For each mutant, the value of k_{cat1} increases as the ionic strength increases. The C*c*P(MI,N34), C*c*P(MI,F193), and C*c*P(MI,N290) enzymes approach a limiting value for k_{cat1} when $\mu > 50$ mM. As k_{cat1} approaches this limiting value, the second kinetic process is no longer detected, and v_0 has a simple hyperbolic dependence upon yC*c*^{II} concentration. The ionic strength dependence of k_{cat1} for the C*c*P(MI,Q32) and C*c*P(MI,Q291) mutants was similar to that observed for C*c*P(MI) (Figure 3), where the value of k_{cat1} increases over the entire ionic strength range examined. The transition to simple hyperbolic kinetics occurs at a lower ionic strength ($\mu > 75$ mM) for C*c*P(MI,Q32) than for C*c*P(MI). The value of k_{cat1} at high ionic strength varied by only 2.5-fold for the mutants, ranging from 900 s^{-1} for C*c*P(MI,N34) to 2300 s^{-1} for C*c*P(MI,Q32).

The effect of mutations on k_{cat2} and K_{m2} are more difficult to analyze, because of the large uncertainty in these parameters. The values of k_{cat2} as well as the bimolecular rate constant k_{cat2}/K_{m2} appear to be 2−3-fold greater for C*c*P(MI,N34), C*c*P(MI,F193), and C*c*P(MI,N290) than for C*c*P(MI), while the values of k_{cat2} and K_{m2} for C*c*P(MI,Q291) are 2-fold smaller than for C*c*P(MI). These differences appear to be statistically significant, and may indicate that the mutations alter the second kinetic process as well as the first.

DISCUSSION

Steady-State Mechanism for CcP(MI). The kinetic results presented here are interpreted in the context of the mechanism shown in Figure 4. It is assumed that reduction of the Trp 191 radical occurs first, followed by reduction of the oxy-ferryl heme. For the purposes of model building,

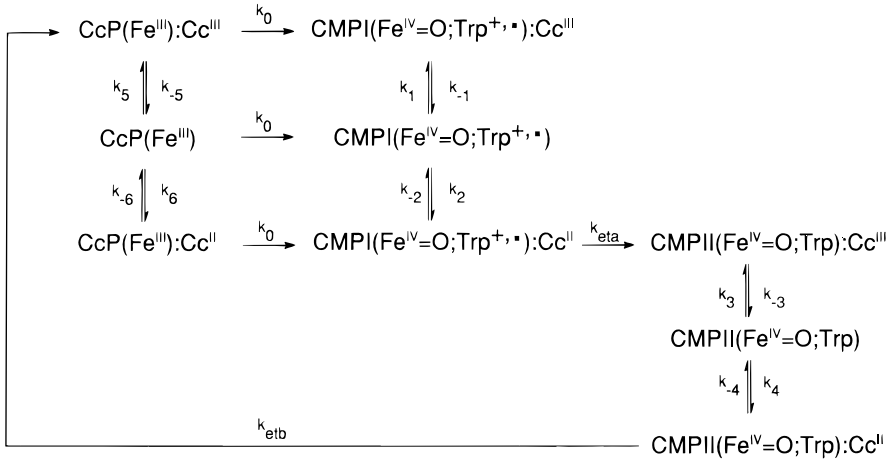

FIGURE 4: Kinetic model for catalysis at the high-affinity site of C*c*P(MI). The rate constants were estimated as described under Discussion.

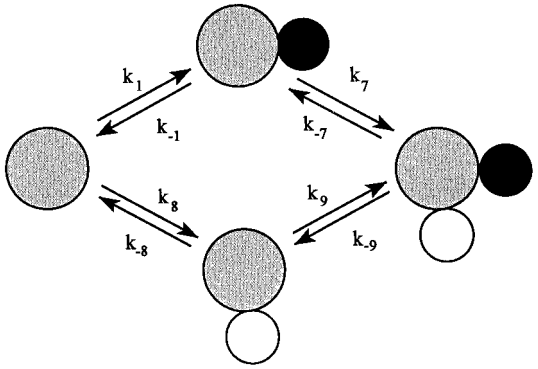

FIGURE 5: Two-binding site model for C*c*P. The gray spheres represent C*c*P, the black spheres represent yC*c* bound at the high-affinity site, and the white spheres represent yC*c* bound at the low-affinity site.

reduction of the Trp 191 radical and the oxy-ferryl heme are adequately represented as simple first-order reactions, with rate constants k_{eta} and k_{etb}, respectively (Wang et al., 1996).

The model shown in Figure 4 is sufficient to account for the data at high ionic strength, where the dependence of v_0 on yC*c*^{II} concentration is adequately described by a simple rectangular hyperbola. The model predicts that $k_{cat1} = k_0k_{etb}/k_0 + k_{etb}$ if yC*c* binding and dissociation are rapid relative to intracomplex ET. The model is not sufficient to account for the non-hyperbolic yC*c*^{II} dependence of v_0 at lower ionic strength ($\mu \leq 90$ mM), however. The data at low ionic strength are best explained by assuming that two (or more) yC*c* binding sites are important in determining the rate of enzyme turnover at lower ionic strength. The existence of a second, low-affinity yC*c* binding site has been demonstrated (Kornblatt & English, 1986; Stemp & Hoffman, 1993; Mauk et al., 1994; Zhou & Hoffman, 1994; Zhou et al., 1995), but this site is unreactive in ET (Miller et al., 1996). The model must therefore include a second, low-affinity binding site that increases enzyme turnover without being reactive in ET.

A mechanism that meets these criteria can be constructed by replacing the one binding site equilibria in Figure 4 with the two binding site equilibria shown in Figure 5. Two additional criteria must be imposed upon the model: (1) formation of the [CMPII(Fe^{IV}=O;Trp):yC*c*^{II}] intermediate must be limited by yC*c*^{III} dissociation from the high-affinity binding site when $\mu \leq 90$ mM and (2) the rate of yC*c*^{III} dissociation from the high-affinity binding site must increase when yC*c*^{II} binds at the low-affinity binding site (i.e., $k_{-1} < k_{-9}$ in Figure 5).

Dissociation of yC*c from the High-Affinity Site Limits Catalysis.* The notion that yC*c*^{II} oxidation is limited by product dissociation at low ionic strength is not new (Kang et al., 1977). To confirm this aspect of the mechanism, it must be shown that k_{cat1} is proportional to k_{-1} rather than k_{etb}. The relationship between k_{-1} and k_{cat1} was examined by using the numerical integration program KINSIM (Barshop et al., 1983) to simulate turnover rates for C*c*P(MI) at the high-affinity binding site. Simulations were based on the mechanism in Figure 4, with two simplifying assumptions. First, the rate of the peroxide reaction was assumed to be unaffected by yC*c* binding at the high-affinity site. It is known that hC*c* binding at the high-affinity site does not alter the peroxide reaction (Hoth & Erman, 1984); given the similarity of the C*c*P(MI):hC*c* and C*c*P(MI):yC*c* complexes (Pelletier & Kraut, 1992) it seems reasonable to assume the same will be true for yC*c*. Second, the dissociation rate for yC*c* was assumed to be unaltered by the oxidation states of yC*c* and C*c*P(MI) (i.e., $k_{-1} = k_{-2} = k_{-3} = k_{-4} = k_{-5} = k_{-6}$ in Figure 4). The effect of yC*c* oxidation state on binding is known to be small (Mauk et al., 1994), but comparable data are not available for C*c*P(MI). The assumption seems reasonable because the heme of C*c*P is at least 17 Å from any surface of the enzyme where yC*c* can bind.

Rate constants for the simulations were obtained from the literature. The bimolecular rate constant for the peroxide reaction is 3.9×10^7 M^{-1} s^{-1} in phosphate buffer (Vitello et al., 1990), which gives a pseudo-first-order rate constant $k_0 = 5850$ s^{-1} at 150 μM HOOH. Rate constants for intracomplex ET were determined using yC*c* labeled with a ruthenium dimethylbipyridine group at position 39 (Ru-39-yC*c*). At pH 7.0, the rate constant k_{eta} decreases from 2×10^6 s^{-1} at $\mu = 5$ mM to 1.2×10^6 s^{-1} at $\mu = 105$ mM and the rate constant k_{etb} decreases from $k_{etb} = 5000$ s^{-1} at $\mu = 5$ mM to $k_{etb} = 3500$ s^{-1} at $\mu = 105$ mM at pH = 7.0 (Wang et al., 1996). Assuming that log k_{eta} and log k_{eta} vary linearly with $(\mu)^{1/2}$, the rate constants were calculated from the following relations: log $k_{eta} = -0.88(\mu)^{1/2} + 6.36$ and log $k_{etb} = -0.61(\mu)^{1/2} + 3.74$. The rate constant k_{-1} between $\mu = 44$ mM and $\mu = 158$ mM is reported in the accompanying paper (Mei et al., 1996). Over this ionic strength range, k_{-1} ($= k_{-2} = k_{-3} = k_{-4} = k_{-5} = k_{-6}$) was estimated from the

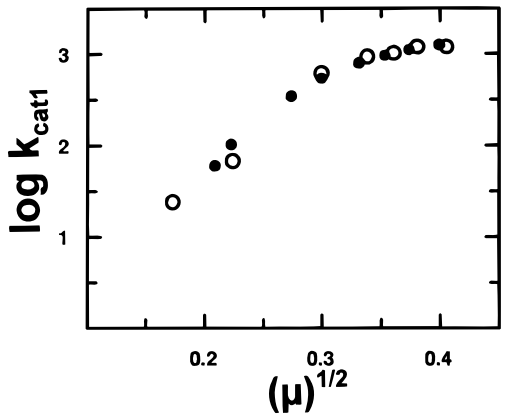

FIGURE 6: Comparison of predicted and observed values of k_{cat1} for yCc^{II} oxidation by C*c*P(MI) at pH 7, 25 °C. Experimental values (open circles) were obtained as described under Experimental Procedures. Predicted values (closed circles) were obtained using the numerical integration program KINSIM. The calculated values were obtained by applying rate constants derived from the literature (see Discussion) to the model in Figure 4.

empirically determined relation $\log k_{-1} = 5.36 - 0.676(\mu)^{-1/2}$. The equilibrium binding constant was estimated as $\log K_{D1} = \log(1.2K_{m1}) = 14(\mu)^{1/2} - 9.77$, on the basis of the relationship between K_{m1}, K_{D1}, and ionic strength between $\mu = 40$ mM and $\mu = 160$ mM at pH 6.0. The value of k_1 ($= k_2 = k_3 = k_4 = k_5 = k_6$) was calculated by assuming a simple binding equilibrium where $K_{D1} = k_{-1}/k_1$.

As shown in Figure 6, the values of k_{cat1} predicted by the model are in excellent agreement with observed values between $\mu = 40$ mM and $\mu = 160$ mM. Thus, the model adequately describes catalysis at the high-affinity site. The model predicts that most of the enzyme exists as CMPI(Fe^{IV}=O;$Trp^{\bullet+}$):yCc^{III} and CMPII(Fe^{IV}=O):yCc^{III} (Figure 4) between $\mu = 20$ mM and $\mu = 90$ mM. Under these conditions, $k_{cat1} \approx k_{-1}k_{-3}/k_{-1} + k_{-3}$. The assumption that the oxidation state of C*c*P(MI) does not influence the rate of yC*c* dissociation seems to hold, since $k_{cat1} \approx k_{-1}/2$ at low ionic strength. As the ionic strength is increased above 90 mM, k_{-1} becomes sufficiently large (e.g., 1900 s^{-1} at $\mu =$ 105 mM) that it is comparable to k_{etb} (3500 s^{-1} at $\mu = 105$ mM) and k_0 (5850 s^{-1}). Under these conditions, the model predicts that yC*c* dissociation will influence the rate of enzyme turnover, but the rate should also be influenced by k_{etb} and k_0.

To test the prediction that k_0 influences enzyme turnover at high ionic strength, the HOOH dependence of v_0 was characterized at $\mu = 200$ mM. As shown in Figure 7, v_0 increases with increasing HOOH concentration, and saturation occurs at greater than 600 μM HOOH. The best fit of the data to a simple rectangular hyperbola gave a maximal turnover rate of 1370 ± 40 s^{-1} and apparent $K_{m1} = 57 \pm 8$ μM when yC$c^{II} = 80$ μM. The results show that k_0 has a significant influence on enzyme turnover rate, as predicted by the model. The value of k_{cat1} in Table 1 represents only ~72% of the maximal turnover rate at $\mu = 200$ mM. Previous studies employing HOOH concentrations of 200 μM or less also underestimate k_{cat1} to the extent that $k_0k_{etb}/k_0 + k_{etb} < k_{etb}$.

In evaluating the model, it is important to note that log k_{-1} and log K_{D1} do not have a linear dependence upon $(\mu)^{1/2}$ (Figure 3B; Mei et al., 1996). Instead, the ionic strength dependencies of k_{-1} (i.e., $\delta k_{-1}/\delta\mu$) and K_{D1} (i.e., $\delta K_{D1}/\delta\mu$) increase as the ionic strength decreases. Data reported by others do not conflict with this conclusion [see Matthis and Erman (1995) for review]. This nonideal behavior is not surprising, since the simple linear relationship between free energy and $(\mu)^{1/2}$ breaks down even for NaCl when $\mu > 10$ mM. Nonideal behavior in the C*c*P:hC*c* system was recognized by Erman and Vitello (1980), who noted that the ionic strength dependence of K_{D1} for C*c*P:hC*c* was significantly weaker than would be predicted, based on the charges on the individual molecules solution.

This observation is important in interpreting the ionic strength dependence of yC*c* binding and dissociation at the high-affinity site. Generally, yC*c* binding is assumed to be a simple process where $K_{D1} = k_{-1}/k_1$, and it is known that k_1 decreases with increasing ionic strength (Liu et al., 1994; Matthis & Erman, 1995; Mei et al., 1996). These observations require that $\delta K_{D1}/\delta\mu > \delta k_{-1}/\delta\mu$. The data are consistent with this prediction. Point by point comparison of K_{D1} and k_{-1} shows that $\delta K_{D1}/\delta\mu \geq \delta k_{-1}/\delta\mu$ over the ionic strength range where both parameters can be determined. On the other hand, $\delta k_1/\delta\mu$ decreases as the ionic strength decreases, presumably because k_1 reaches a limiting value at low ionic strength.

Although the model adequately describes the ionic strength dependence of enzyme turnover at pH 7.0, it should be noted that enzyme turnover has a pH dependence that has not yet been built into the model. When $\mu \leq 90$ mM, the values of k_{cat1} are 1.3-fold smaller at pH 7.0 than at pH 6.0 and 7.5 (Figure 6, Table 2; Matthis & Erman, 1995). It seems likely that k_{-1} is 1.3-fold greater at pH 6.0 and 7.5 than at pH 7.0, since K_{D1} reaches its minimum value at pH 7.0 (Mauk et al., 1994). The pH dependence observed at high ionic strength cannot be explained in the context of changes in k_{-1}, however. When $\mu \geq 160$ mM, k_{cat1} decreases monotonically from 2200 s^{-1} at pH 6.0 to 880 s^{-1} at pH 7.5, instead of reaching a minimum value at pH 7.0 (Figure 6; Matthis & Erman, 1995). Given that k_0 is independent of pH and ionic strength (Vitello et al., 1990), the pH dependence at high ionic strength may be caused by a weak pH dependence of k_{etb} and/or a pH-dependent change in the ratio k_{-1}/k_{-3}.

Role of the Low-Affinity yCc Binding Site in Catalysis

The accompanying paper presents evidence that the rate of yC*c* dissociation from the high-affinity site increases when yC*c* binds at the low-affinity site (Mei et al., 1996). This satisfies the second requirement of the two-site model and provides a molecular interpretation for the "substrate-assisted displacement" observed by others (Satterlee et al., 1992; McLendon et al., 1993; Corin et al., 1993; Yi et al., 1994). The bimolecular rate constants estimated by others ($1.0-1.8 \times 10^6$ M^{-1} s^{-1} at $\mu = 10$ mM; McLendon et al., 1993; Yi et al., 1994) are comparable to the value of 1.7×10^6 M^{-1} s^{-1} for C*c*P(MI) between $\mu = 40$ mM and $\mu = 90$ mM (Table 2).

According to the two-site model, the rate constant for yCc^{III} dissociation from the high-affinity site (k_{off}) is given by

$$k_{off} = k_{-1}[CcP{:}yCc]/CcP_{tot} + k_{-9}[CcP{:}yCc_2]/CcP_{tot} \quad (7)$$

where $[CcP{:}yCc]/CcP_{tot}$ is the mole fraction of the enzyme

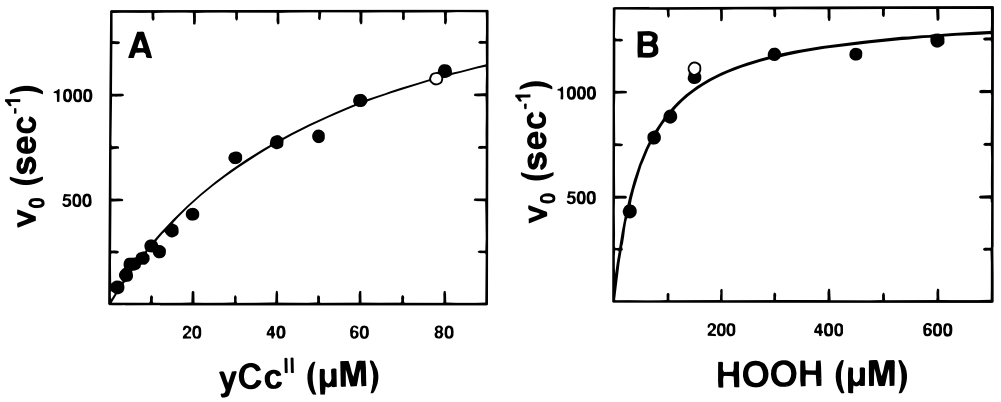

FIGURE 7: Dependence of v_0 upon yC*c*^{II} and HOOH concentration at $\mu = 200$ mM, pH 6.0. (A) yC*c*^{II} dependence of v_0; HOOH concentration = 150 μM. (B) HOOH dependence of v_0; yC*c*^{II} concentration = 80 μM. The solid lines represent the best fit of the data to a simple rectangular hyperbola; the parameters are $k_{cat1} = 2000$ s^{-1} and $K_{m1} = 65$ μM (panel A); $k_{cat1} = 1374$ s^{-1} and $K_{m1} = 57$ μM. (panel B). The open circles show data from the adjacent panel that were collected under comparable conditions. These are included to indicate reproducibility between experiments.

in the 1:1 complex with yC*c* bound at the high-affinity site and [C*c*P:yCc_2]/C*c*P$_{tot}$ is the mole fraction of the 1:2 complex with yC*c* bound at both sites.[3] At low yC*c*^{II} concentrations, C*c*P:yC$c_2 \approx 0$, and $k_{off} \approx k_{-1}$. Under these conditions, v_0 will obey a hyperbolic dependence on yC*c*^{II} concentration, where k_{cat1} is proportional to k_{-1}. With increasing yC*c*^{II} concentrations, the mole fraction of the 1:2 complex increases, and the second term in eq 7 becomes significant. This will cause the yC*c*^{II} dependence of v_0 to deviate from simple hyperbolic kinetics. At very high yC*c* concentrations, all of the enzyme will be converted to the C*c*P:yCc_2 complex, and $k_{off} \approx k_{-9}$.

The two-site model accounts for the change in yC*c*^{II} dependence of v_0 with ionic strength. At $\mu > 90$ mM, the hyperbolic dependence described by K_{m1} and k_{cat1} indicates that catalysis is predominantly by the 1:1 complex. Thus, although k_{-1} is partially limiting, the low-affinity site has a very low occupancy at $\mu > 90$ mM under the conditions of the experiments (Mei et al., 1996; Mauk et al., 1994). At $\mu \leq 90$ mM, a linear yC*c*^{II} dependence is observed in addition to the hyperbolic process because a fraction of enzyme is present as the 1:2 complex and [yC*c*^{II}] $\ll K_{m2}$; therefore the mole fraction of the 1:2 complex increases linearly with increasing yC*c*^{II} concentration up to 80 μM yC*c*^{II}. Under these conditions, the apparent rate of the second process is $\sim k_{cat2}/K_{m2}$, which is proportional to $k_{-9}k_7/k_{-7}$ (Figure 5). When $\mu < 50$ mM, catalysis by the 1:1 C*c*P(MI):yC*c* complex saturates at less than 1 μM yC*c*^{II} and saturation of the low-affinity site can also be detected in the concentration range of the experiment when $\mu < 40$ mM. Under these conditions, the model predicts that the apparent K_{m2} is proportional to k_{-7}/k_7 while k_{cat2} is proportional to k_{-9}. It is interesting to note that the slope of the line describing the second process ($k_{-9}k_7/k_{-7}$) does not have a strong dependence upon ionic strength. This is presumed to indicate that k_{-9} and k_{-7} have a similar dependence upon ionic strength.

The strength of the interaction between the two binding sites can be estimated by assuming $k_{cat2} \approx 0.5k_{-9}$ and $k_{cat1} \approx 0.5k_{-1}$. At $\mu = 20$ mM, $k_{cat2}/k_{cat1} = 64$, which means the affinity for yC*c* at the high-affinity site will decrease 64-fold if the bimolecular rate of binding is unchanged (i.e., $k_1 = k_9$, Figure 5). The model requires that binding at the high-affinity site weakens binding at the low-affinity site as well. Thus, at $\mu = 20$ mM, the equilibrium binding constant for the low-affinity site (K_{D2}) must increase 64-fold when the high-affinity site is occupied. Assuming that $K_{m2} \approx K_2$, then $k_{-8}/k_8 = K_{m2}/(k_{cat2}/k_{cat1}) = 122$ μM/64 = 1.9 μM.

Effect of Mutations on Enzyme Turnover

The effect of the mutations on enzyme turnover can also be explained in the context of the two binding site model. All of the mutations increase the value of k_{cat1}; the greatest increases (27−38-fold at $\mu = 20$ mM) are observed for C*c*P(MI,N290), C*c*P(MI,N34), and C*c*P(MI,F193), while the smallest increase (3-fold at $\mu = 20$ mM) is observed for C*c*P(MI,Q291). A similar trend is observed for the effect of the mutations on k_{-1} (Mei et al., 1996). Together, the data support the interpretation that enzyme turnover is controlled by the rate of yC*c* dissociation at low ionic strength.

The model also makes it possible to interpret the effect of mutations on the transition from two kinetic processes to a single hyperbolic process. This transition occurs at $\mu = 110$ mM for C*c*P(MI), but the Asp 34 → Asn and Ala 193 → Phe mutations shift the transition to $\mu < 50$ mM. The model identifies two possible causes for this transition: (1) binding of yC*c* at the low-affinity site becomes very weak, or (2) the rate-limiting step changes from yC*c* dissociation to intracomplex ET. Since these mutations are not expected to alter binding at the low-affinity site, changes in the rate-limiting step seem more likely.

The data support this conclusion. For both C*c*P(MI,N34) and C*c*P(MI,F193), the value of k_{cat1} reaches a maximum between $\mu = 50$ mM and $\mu = 110$ (Figure 3A), and at $\mu = 110$ mM, $k_{cat1} \approx k_{etb}$. These observations indicate that the transition to simple hyperbolic kinetics for C*c*P(MI,N34) and C*c*P(MI,F193) occurs because turnover is limited by the rate

[3] The fraction of C*c*P present as the 1:1 and 1:2 complexes is given by eq 8 (below).

$$\frac{\text{C}c\text{P:yC}c}{\text{C}c\text{P}_{tot}} = [\text{yC}c^{II}]/\{K_{m1} + [\text{yC}c^{II}] + ([\text{yC}c^{II}]^2/K_{m2})\};$$

$$\frac{\text{C}c\text{P:yC}c_2}{\text{C}c\text{P}_{tot}} = [\text{yC}c^{II}]/\{K_{m2} + [\text{yC}c^{II}] + (K_{m1}K_{m2}/[\text{yC}c^{II}])\} \quad (8)$$

Parameters derived from fits of the data to eq 8 were identical (within the error of the experiments) to parameters derived from eq 6, which indicates that the denominator terms $[\text{yC}c^{II}]^2/K_{m2}$ and $K_{m1}K_{m2}/[\text{yC}c^{II}]$ are negligible.

of intracomplex ET rather than yC*c* dissociation. In contrast, the values of k_{cat1} for C*c*P(MI,Q32), C*c*P(MI,Q291), and C*c*P-(MI) increase significantly between $\mu = 50$ mM and $\mu =$ 110 mM. At $\mu = 110$ mM, the values of k_{cat1} for C*c*P(MI,-Q32), C*c*P(MI,Q291), and C*c*P(MI) are 52%, 35%, and 24% of k_{etb}, respectively. For these enzymes, turnover is still partially limited by k_{-1} at $\mu = 110$ mM, and the transition to simple hyperbolic kinetics occurs because binding of yC*c* to the low-affinity site is very weak at this ionic strength.

The two site model also explains the effect of a bulky derivative at position 193 on the kinetics of yC*c*^{II} oxidation. When 3-(*N*-maleimidylpropionyl)biocytin (MPB) is attached at position 193 of C*c*P(MI,C193), the intracomplex ET rate (k_{eta}) decreases substantially, and the binding constant for yC*c* at the high-affinity site increases (Miller et al., 1996). If it is assumed that $k_{-1} \geq 360$ s^{-1} for this enzyme (the value observed at $\mu = 20$ mM when Ala 193 is replaced by Phe), numerical integration predicts that the MPB-mutant will exhibit simple hyperbolic kinetics with $k_{cat1} = 38$ s^{-1}. Because $k_{cat1} \ll k_{-1}$, k_{cat1} is predicted to be independent of ionic strength. In good agreement with the model, the data for MPB-C*c*P(MI,C193) show that $k_{cat1} = 32$ s^{-1}, independent of ionic strength (Miller et al., 1996). An interesting consequence of the interaction between the two binding sites is that when $k_{etb} \ll k_{-1}$, binding at the low-affinity site will not increase k_{cat1}, but should cause an increase in the apparent K_{m1}. This effect is not observed for C*c*P(MI) because $k_{etb} \ll k_{-1}$ only at high ionic strength, where binding at the low-affinity site is not detected under current experimental conditions. However, for MPB-C*c*P(MI,C193), $k_{etb} \ll k_{-1}$ at $\mu = 20$ mM, where the low-affinity site is occupied when yC*c*$^{II} \leq 80$ μM. The apparent K_{m1} for yC*c*^{II} increases from 8 to 16 μM as the ionic strength decreases from 30 to 20 mM (Miller et al., 1996), in good agreement with the model.

Relationship to Previous Studies

The model presented here accounts for the presence of two yC*c* binding sites that differ vastly in their affinity for yC*c* (Kornblatt & English, 1986; Stemp & Hoffman, 1993; Mauk et al., 1994; Zhou & Hoffman, 1994, 1995). It also accounts for the observation that both sites can influence the catalytic rate at low ionic strength (Matthis & Erman, 1995; Wang & Margoliash, 1995; present work), although only one site is reactive in intramolecular ET (Miller et al., 1996). It explains the dependence of the ET reaction on the presence of a readily oxidized Trp 191 near the heme (Miller et al., 1995; Millett et al., 1995; Mauro et al., 1988; Bonagura et al., 1996) and supports the high-affinity binding site observed in the crystal structure of the C*c*P(MI):yC*c* complex (Pelletier & Kraut, 1992).

Although the agreement between model and experiment is substantial, it is important to acknowledge that data from several previous studies appear to conflict with the present model. On the basis of stopped-flow measurements of the reaction between compound I and yC*c*^{II} (Matthis et al., 1995; Nuevo et al., 1993; Summers & Erman, 1988), Matthis and Erman (1995) proposed that ET occurs at both high- and low-affinity binding sites and that ET at the low-affinity site predominates at low ionic strength. This interpretation is incompatible with the observation that both high and low K_m processes are altered by single-site mutations (Figure 2; Tables 1 and 2). It is also incompatible with the observation that covalent modification at position 193 of C*c*P(MI,C193) dramatically alters both high- and low-affinity processes (Miller et al., 1996). Moreover, recent work by others (Wang et al., 1996) suggests that the discrepancy may be the result of a technical problem with the stopped-flow measurements.

Matthis and Erman (1995) also concluded that enzyme turnover at the high-affinity site is limited by a conformational change rather than yC*c* dissociation, because the value of $k_{-1} = 187$ s^{-1} estimated from NMR data (Yi et al., 1994) was much larger than the rate of turnover at $\mu = 10$ mM ($k_{cat1} = 4$ s^{-1}). The value of k_{-1} calculated from NMR data employed only two concentrations of yC*c*, however, and the error inherent in this calculation is significant. Mei et al. (1996) report that $k_{-1} < 5$ s^{-1} and $K_{D2} = k_{-7}/k_7 = 65$ μM at $\mu = 5$ mM. The latter two values, together with the NMR data, predict that $k_{-9} \approx 890 \pm 30$ s^{-1}, in reasonable agreement with the value $k_{-9} = 600 \pm 200$ s^{-1} reported by Mei et al. (1996). The lower value of k_{-1} is also supported by the data of McLendon et al. (1993) using techniques that provide greater precision.

Despite the discrepancies between the two models, the steady-state parameters for oxidation of yC*c*^{II} by C*c*P(MI) (Tables 1 and 2) are quite similar to values reported for bakers' yeast C*c*P in phosphate/nitrate buffer at pH 7.5 (Erman et al., 1991; Matthis & Erman, 1995). The substrate dependence of v_0 is distinctly non-hyperbolic for both enzymes when 20 mM $< \mu <$ 110 mM. The similarities between the two data sets indicate that the mechanism does not depend upon the precise buffer composition or pH. Moreover, the similar kinetic behavior of C*c*P(MI) and C*c*P indicates that the sequence differences [Gly 152 for C*c*P(MI) vs Asp for C*c*P, and Ile 53 for C*c*P(MI) vs Thr for C*c*P] do not have a dramatic effect on enzyme turnover rates.

The results of Hazzard et al. (1987, 1988a,b) are also difficult to interpret in the context of the present model. These experiments used photolysis of flavin semiquinones to generate a small quantity of yC*c*^{II} in the presence of excess compound I. Because compound I is present is molar excess, the experiments should measure only the initial site of compound I reduction. The difference absorption spectrum for this reaction indicates that these experiments measure reduction of the oxy-ferryl heme (Hazzard et al., 1987) rather than Trp$^{\bullet+}$ as would be predicted by the present model. Further experimentation will be required to reconcile these observations with the results obtained by others (Wang et al., 1996; Pappa et al., 1996).

Studies employing chemically cross-linked C*c*P:yC*c* complexes have also been interpreted in the context of two reactive ET sites (Wang & Margoliash, 1995; Pappa & Poulos, 1995). The results can be reconciled with the present model by assuming that free rotation about single bonds in the cross-linking groups can expose the high affinity site of C*c*P. The "high K_m" kinetic process observed for cross-linked C*c*P:yC*c* (Wang & Margoliash, 1995) may indicate that yC*c* binding at the low-affinity site increases the rate of yC*c* rotation away from the high-affinity binding site in cross-linked C*c*P:C*c* complexes.

Evolutionary Implications for Physiological Electron Transfer

The model presented here predicts that the C*c*P:yC*c* complex is optimized both for efficiency of intracomplex ET *and* stability. ET efficiency is optimized by adjusting the orientation of the two partners to achieve maximal

intracomplex ET rates. The data indicate that rapid ET from yC*c*^{II} to compound I occurs at only one site (Miller et al., 1996), and that this site is correctly identified by the crystal structure of the C*c*P(MI):yC*c* complex (Pelletier & Kraut, 1992). Intracomplex ET to the compound I radical remains rapid even at low ionic strength (Geren et al., 1991; Millett et al., 1995), which suggests that the orientation of the two partners does not change significantly with ionic strength. Reduction of the oxy-ferryl heme becomes slow at low ionic strength because product dissociation from the high-affinity site is slow, but not because pairing between C*c*P and yC*c* is imperfect, as was previously thought (Hazzard et al., 1987; 1988a,b; Summers & Erman, 1988; Nuevo et al., 1993; Matthis et al., 1995). Complex stability is optimized by balancing the need for a stable 1:1 complex against the need for rapid product dissociation. Oxidation of yC*c*^{II} by C*c*P is optimal at physiological ionic strength (Tollin et al., 1993) and falls off steeply at lower ionic strength where yC*c*^{III} dissociation becomes rate-limiting. Thus, evolution has made the C*c*P:yC*c* complex as stable as possible without causing product dissociation to limit enzyme turnover. The low-affinity binding site contributes to catalysis only by increasing the rate of yC*c*^{III} dissociation from the reactive high-affinity site. The evolutionary significance of this site remains unclear, since it has little influence on enzyme turnover at physiological ionic strength.

ACKNOWLEDGMENT

This publication is dedicated to Dr. William B. Roess in honor of his 30 years of teaching excellence. The author is grateful to Sunny Kim for outstanding technical assistance and to Hongkang Mei, Bill Durham, and Francis Millett for making data available prior to its publication.

REFERENCES

Barshop, B. A., Wrenn, R. F., & Frieden, C. (1983) *Anal. Biochem. 130*, 134−145.

Bevington, P. R., & Robinson, D. K. (1992) in *Data Reduction and Error Analysis for the Physical Sciences*, McGraw-Hill, New York.

Bonagura, C. A., Sundaramoorthy, M., Pappa, H., Patterson, W., & Poulos, T. L., (1996) *Biochemistry 35*, 6107−6115.

Corin, A., Hake, R. A., McLendon, G., Hazzard, J. T., Tollin, G. (1993) *Biochemistry 32*, 2756−2762.

English, A. M., & Tsaprailis, G. (1995) *Adv. Inorg. Chem. 43*, 79−125.

Erman, J. E., & Vitello, L. B. (1980) *J. Biol. Chem. 255*, 6224−6227.

Ferrer, J. C., Turano, P., Banci, L., Bertini, I., Morris, I. K., Smith, K. M., Smith, M., Mauk, A. G. (1994) *Biochemistry 33*, 7819−7829.

Finzel, B. C., Poulos, T. L., & Kraut, J. (1984) *J. Biol. Chem. 259*, 13027−13036.

Fishel, L. A., Villafranca, J. E., Mauro, J. M., & Kraut, J. (1987) *Biochemistry 26*, 351−360.

Geren, L., Hahm, S., Durham, B., & Millett, F. (1991) *Biochemistry 30*, 9450−9457.

Hahm, S., Durham, B., & Millett, F. (1992) *Biochemistry 30*, 3472−3477.

Hahm, S., Durham, B., & Millett, F. (1993) *J. Am. Chem. Soc. 115*, 3372−3373.

Hahm, S., Miller, M. A., Geren, L., Kraut, J., Durham, B., & Millett, F. (1994) *Biochemistry 33*, 1473−1480.

Hazzard, J. T., Poulos, T. L., & Tollin, G. (1987) *Biochemistry 26*, 2836−2848.

Hazzard, J. T., McLendon, G., Cusanovich, M., Das, G., Sherman, F., & Tollin, G. (1988a) *Biochemistry 27*, 4445−4451.

Hazzard, J. T., McLendon, G., Cusanovich, M., & Tollin, G. (1988b) *Biochem. Biophys. Res. Commun. 151*, 429−434.

Ho, P. S., Hoffman, B. M., Solomon, N., Kang, C. H., & Margoliash, E. (1984) *Biochemistry 23*, 4122−4128.

Hoth, L. R., & Erman, J. E. (1984) *Biochim. Biophys. Acta 788*, 151−153.

Kang, C. H., Ferguson-Miller, S., & Margoliash, E. (1977) *J. Biol. Chem. 252*, 919−926.

Kornblatt, J. A., & English, A. M. (1986) *Eur. J. Biochem. 155*, 505−511.

Liu, R. Q., Hahm, S., Miller, M. A., Durham, B., & Millett, F. (1995) *Biochemistry 34*, 973−983.

Liu, R.-Q., Miller, M. A., Han, G. W., Hahm, S., Geren, L., Hibdon, S., Kraut J., Durham, B., & Millett, F. (1994) *Biochemistry 33*, 8678−8685.

Marquardt, D. W. (1963) *J. Soc. Ind. Appl. Math. 11*, 431−441.

Matthis, A., & Erman, J. E. (1995) *Biochemistry 34*, 9985−9990.

Matthis, A., Vitello, L. B., & Erman, J. E. (1995) *Biochemistry 34*, 9991−9999.

Mauk, M. R., Ferrer, J. C., & Mauk, A. G. (1994) *Biochemistry 33*, 12609−12614.

Mauro, J. M., Fishel, L. A., Hazzard, J. T., Meyer, T. E., Tollin, G., Cusanovich, M. A., & Kraut, J. (1988) *Biochemistry 27*, 6243−6256.

McLendon, G., Zhang, Q., Wallin, S. A., Miller, R. M., Billstone, V., Spears, K. G., & Hoffman, B. M. (1993) *J. Am. Chem. Soc. 115*, 3665−3669.

Mei, H., Wang, K., McKee, S., Pielak, G. J., Durham, B., & Millett, F. (1996) *Biochemistry 35*, 15800−18806.

Miller, M. A., Liu, R.-Q., Hahm, S., Geren, L., Hibdon, S., Kraut, J., Durham, B., & Millett, F. (1994) *Biochemistry 33*, 8686−8693.

Miller, M. A., Erman, J. E., & Vitello, L. B. (1995) *Biochemistry 34*, 12048−12058.

Miller, M. A., Geren, L., Han, G. W., Saunders, A., Pielak, G., Durham, B., Millett, F., & Kraut, J. (1996) *Biochemistry 35*, 667− 673.

Millett, F., Miller, M. A., Geren, L., & Durham, B. (1995) *J. Bioenerg. Biomembr. 27*, 341−351.

Moench, S. J., Chroni, S., Lou, B.-S., Erman, J. E., & Satterlee, J. D. (1992) *Biochemistry 31*, 3661−3670.

Nuevo, M. R., Chu, H.-H., Vitello, L. B., & Erman, J. E. (1993) *J. Am. Chem. Soc. 115*, 5873−5874.

Pappa, H. S., & Poulos, T. L. (1995) *Biochemistry 34*, 6573−6580.

Pappa, H. S., Tajbaksh, S., Saunders, A., Pielak, G. J., & Poulos, T. L. (1996) *Biochemistry 35*, 4837−4845.

Pelletier, H., & Kraut, J. (1992) *Science 258*, 1748−1755.

Roe, J. A., & Goodin, D. B. (1993) *J. Biol. Chem. 268*, 20037−20045.

Satterlee, J., Moench, S., Chroni, S., Lou, B. S., & Erman, J. (1992) *Biochemistry 31*, 3661−3670.

Stemp, E. D. A., & Hoffman, B. M. (1993) *Biochemistry 32*, 10848−10865.

Summers, F. E., & J. E. Erman (1988) *J. Biol. Chem. 263*, 14267−14275.

Tollin, G., Hurley, J. K., Hazzard, J. T., & Meyer, T. E. (1993) *Biophys. Chem. 48*, 259−279.

Vitello, L. B., & Erman, J. E. (1987) *Arch. Biochem. Biophys*. 258, 621−629.

Vitello, L. B., Erman, J. E., Mauro, J. M., & Kraut, J. (1990) *Biochim. Biophys. Acta 1038*, 90−97.

Vitello, L. B., Erman, J. E., Miller, M. A., Mauro, J. M., & Kraut, J. (1992) *Biochemistry 31*, 11524−11535.

Wang, Y., & Margoliash, E. (1995) *Biochemistry 34*, 1948−1958.

Wang, K., Mei H., McKee, S., Pielak, G. J., Durham, B., & Millett, F. (1996) Biochemistry *in press*.

Yi, Q., Erman, J. E., & Satterlee, J. D. (1994) *J. Am. Chem. Soc. 116*, 1981−1987.

Zhou, J., & Hoffman, B. M. (1994) *Science 265*, 1693−1696.

Zhou, J. S., Nocek, J. M., DeVan, M. L., & Hoffman, B. M. (1995)- *Science 269*, 204−207.

BI961488C